

PACS numbers: 52.38.Kd, 52.70.Nc, 52.77.Bn
DOI: 10.1070/QE2003v033n11ABEH002534

Formation of the ion current of a high-temperature femtosecond laser plasma on the target surface containing an impurity layer

R.V. Volkov, D.M. Golishnikov, V.M. Gordienko, M.S. Dzhidzhoev, I.M. Lachko, B.V. Mar'in, P.M. Mikheev, A.B. Savel'ev, D.S. Uryupina, A.A. Shashkov

Abstract. **The effect of an impurity film lying on the surface of a target in a vacuum of up to 10^{-5} Torr on the ion acceleration in a plasma, which is formed by a 2×10^{16}-W cm^{-2} femtosecond laser pulse is studied using the time-of-flight and mass spectrometry techniques. It is shown that, under such conditions, the maximum mean energy per unit charge (8 keV) is gained by protons, whereas the ions constituting the target substance (Si, Ti) acquire an energy per unit charge of < 1 keV. The use of a < 10 J cm^{-2} nanosecond laser pulse applied 0.1–100 ms before a femtosecond laser pulse allows the target surface to be efficiently cleaned due to the removal of H-, C-, and O-containing molecules from it. Unlike a continuous thermal heating of a surface, the pulse laser cleaning ensures higher heating temperatures and can be efficiently applied to any solid targets in both the thermal and plasma cleaning modes.**

Keywords: *femtosecond laser plasma, laser cleaning of targets.*

1. During experiments with a high-temperature plasma formed on the surface of a solid target by femtosecond laser pulses, a typical residual pressure in the interaction chamber is $10^{-3} - 10^{-5}$ Torr. Under such conditions, an impurity layer with a thickness of $l \sim 1 - 10$ nm is always present at the target surface. This thickness is comparable to that of a hot plasma layer $\sim 30 - 100$-nm thick [1–6] ($l \sim 2$ nm for hydrocarbon compounds at an Au surface [7] and for an oxide at a Si surface [8]). The presence of such a layer leads to a substantially modified spectrum of the ion plasma component, which is especially important when studying the plasma using the time-of-flight and mass spectrometry techniques [1, 2, 9, 10]. These diagnostic methods allow one to evaluate the ion energy and plasma charge composition. This is important, in particular, for predicting the efficiency of initiating a D–D fusion reaction on modified solid-target surfaces exposed to femtosecond laser radiation [11].

To exclude a spurious effect of surface contaminants, a thermal cleaning technique, at which a surface is resistively heated by 500–1500 °C, can be used. This temperature is sufficient for breaking the bonds of hydrocarbon molecules with the surface and activating the process of impurity desorption from the near-surface target layer to vacuum. The desorption time of thermally unstable compounds is usually short ($10^{-13} - 10^{-6}$ s) and allows the use of both continuous [3, 12, 13] and pulsed [14, 15] surface-heating modes. The resistive technique is applicable only to metal targets or targets with a nonconducting layer deposited on a conducting substrate, whose heating by several hundred degrees does not result in an upper-layer exfoliation.

Pulsed laser radiation is efficiently used to clean surfaces [14–17]. Although pulsed laser cleaning of surfaces of various materials has been long known [8], it is pointed out in Ref. [3] that researchers failed to prepare a clean target surface for studying the parameters of a high-temperature plasma produced by a femtosecond laser pulse.

This work shows that the ion spectrum and the ion acceleration in a plasma, which is produced by a 2×10^{16}-W cm^{-2} femtosecond laser pulse on a solid target surface placed in a vacuum at a residual pressure of 10^{-5} Torr, are distorted due to the presence of surface impurity and oxide layers containing hydrogen, carbon, and oxygen atoms. It was established in our experiments that the protons accelerated by the hot electron component gain the highest mean energy per unit charge, whereas the ions of the target substance are accelerated at the expense of the thermal electron component. The measurements performed in a two-pulse regime, when the first pulse heated (cleaned) the surface and the second one, delayed by a certain time, formed a high-temperature plasma, have shown a significant decrease in the fractions of H, C, and O impurity ions relative to the ions of the target base material.

2. The experimental setup (Fig. 1) included a femtosecond laser facility that produced an intensity of 10^{16} W cm^{-2} for a focused beam, a vacuum interaction chamber, and a pulsed cleaning laser. Two types of targets (Si and Ti) were used in experiments, because we had accumulated a large amount of experimental data on the properties of plasma formed by a femtosecond laser pulse at targets of these materials, including the data obtained by the time-of-flight and mass spectrometry techniques [1, 2, 18–22]. A target was placed in the vacuum chamber with a minimum residual-gas pressure of 3×10^{-5} Torr, which was determined by both the capabilities of the vacuum chamber in use

R.V. Volkov International Teaching and Research Laser Center, Moscow State University, Vorob'evy gory, 119992 Moscow, Russia;
D.M. Golishnikov, V.M. Gordienko, M.S. Dzhidzhoev, I.M. Lachko, P.M. Mikheev, A.B. Savel'ev, D.S. Uryupina, A.A. Shashkov Moscow State University, Department of Physics, Vorob'evy gory, 119992 Moscow, Russia;
B.V. Mar'in D.V. Skobel'tsyn Institute of Nuclear Physics, Moscow State University, Vorob'evy gory, 119992 Moscow, Russia

Received 22 May 2003; revision received 4 September 2003
Kvantovaya Elektronika **33** (11) 981–986 (2003)
Translated by A.S. Seferov

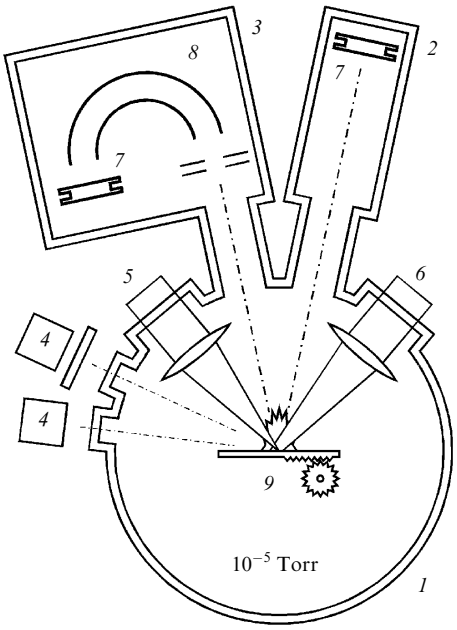

Figure 1. Schematic of the experimental setup: (*1*) interaction chamber; (*2*) time-of-flight measurement chamber; (*3*) mass-spectrometry measurement chamber; (*4*) X-ray detectors (NaI) with filters; (*5*) plasma-generating femtosecond pulse radiation; (*6*) cleaning pulse radiation; (*7*) VEU-7 detectors; (*8*) electrostatic-field mass spectrometer; (*9*) movable target.

and the minimum pressure necessary for the operation of a microchannel-plate ion detector.

Gas-discharge pulsed CO_2 ($\lambda_c = 10.6$ μm, the pulse energy is $E = 30$ mJ, the pulse duration is $\tau \approx 100$ ns) and XeCl ($\lambda_c = 0.308$ μm, $E = 10$ mJ, and $\tau \approx 30$ ns) lasers were used to clean the surfaces of solid targets. During laser cleaning, laser radiation was focused to the target surface at an angle of 45° to produce the energy density $W \sim 10-20$ J cm^{-2} using lenses with a focal length $F = 24$ cm ($\lambda_c = 0.308$ μm with a focal spot 250 μm in diameter) or $F = 50$ cm ($\lambda_c = 10.6$ μm with a focal spot 500 μm in diameter). This energy-density value (and the corresponding intensity $I \sim 10^8$ W cm^{-2}) is obviously higher than the metal-surface breakdown thresholds for nanosecond laser pulses available from the literature [23]. A lower energy density in our experiments was obtained by shifting the lens from the exact-focusing position along the beam axis to the target.

The target surface was also irradiated by p-polarised femtosecond radiation from a dye laser ($\lambda_{fs} = 0.616$ μm, $E \sim 0.5$ mJ, $\tau \approx 200$ fs) [18] incident on the target surface at an angle of 45° (normally to the nanosecond laser beam). The maximum intensity at the target was $I \sim 4 \times 10^{16}$ W cm^{-2}. The delay of the femtosecond pulse relative to the nanosecond pulse was determined by the electronic trigger circuit and measured with a digital oscilloscope, at which a signal from a photodetector registering a nanosecond laser pulse and an electric pulse leading the femtosecond laser pulse by 980 ± 10 ns arrived. The delay between the pulses of the heating (nanosecond) and plasma-initiating (femtosecond) laser systems could be continuously varied from 0 to 400 ns and from 50 μs to 100 ms. After each irradiation, the target was displaced in order to ensure the interaction of laser radiation with a nonperturbed target-surface area in the next measurement. The focusing of a femtosecond laser pulse to the target was controlled by measuring the yields of hard X-rays from plasma simultaneously in two spectral ranges. This also allowed measurements of the mean energy of the hot electron plasma component in each experimental configuration [19].

The target-surface cleaning efficiency was estimated from the ion current of the plasma generated by the femtosecond laser pulse. For this purpose, we used two techniques that are hereafter referred to as time-of-flight and mass spectrometric measurements. The former ensured the measurement of the entire energy spectrum of plasma ions from the ion-current pulse profile for each femtosecond laser pulse, but the atomic-mass and particle-charge resolutions were not provided. The mass spectrometry technique made it possible to simultaneously measure the time of flight for each sort of particles and obtain information on the atomic and charge spectra of ions. However, to obtain the complete ion energy spectrum using this technique, several hundreds of femtosecond laser pulses were required. The energy, mass, and charge resolutions for the detected ions were achieved in the latter technique by using an electrostatic spectrometer in the form of a cylindrical capacitor with a particle-beam rotation angle of 180°. The analysing voltage at the plates of this capacitor could be varied from 0.1 to 8 kV, thus ensuring the detection of particles with energies of 0.4–35 keV per unit charge. The principles of the spectrometer operation and calibration are described in detail in Ref. [2].

Figure 1 shows a schematic of the experiment. Depending on the technique used, one of the detection chambers was joined to the interaction chamber. The plasma ion current was detected along the normal to the target surface. In both cases, the ion current was measured by a VEU-7 detector with a 50-Ω load using a digital oscilloscope with a passband of 100 MHz. The distance between the target and detector was 21 and 62 cm (25 cm of them in the field of the cylindrical capacitor) for the time-of-flight and mass spectrometric measurements, respectively.

3. In the first run of experiments, we compared the ion spectra obtained using the time-of-flight and mass spectrometry techniques for Si and Ti targets that were not exposed to laser cleaning. A typical form of the signal obtained using the mass spectrometry technique at an analysing voltage $U = 400$ V is shown in Fig. 2a for the Ti target. The time position of a peak is related to the parameter M/Z (the particle mass-to-charge ratio) as

$$\Delta t = l\left(\frac{M}{Z}\right)^{1/2}\left(\frac{1}{4.2U}\right)^{1/2}. \quad (1)$$

Thus, the parameter M/Z and, consequently, the atomic number for a given peak can be determined at a fixed U value. Apart from the peaks corresponding to the detection of Ti ions with a degree of ionisation of 1–4, several peaks corresponding to the detection of H, C, and O ions with various degrees of ionisation are clearly seen. Such signals were obtained over the entire accessible range of analysing voltages U, which allowed us to reconstruct the energy, charge, and atomic spectra of the plasma ion current (averaged over 500 measurements).

The signals obtained with the time-of-flight technique are shown in Figs 3a and 3b for both targets. Their characteristic feature is the presence of two peaks corre-

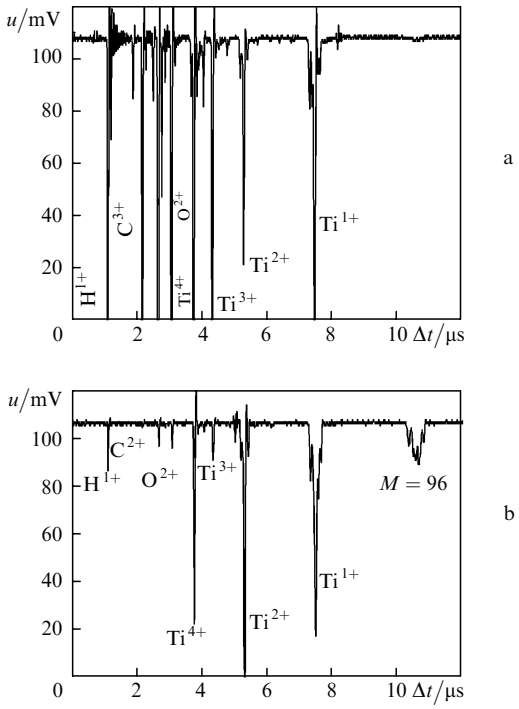

Figure 2. Signals detected by the mass spectrometry technique [Ti target, the ion energy (in keV) is $1.7Z$] (a) without a preliminarily cleaning the target by the XeCl laser pulse and (b) with such a cleaning (the advance time is $t = 90$ ns).

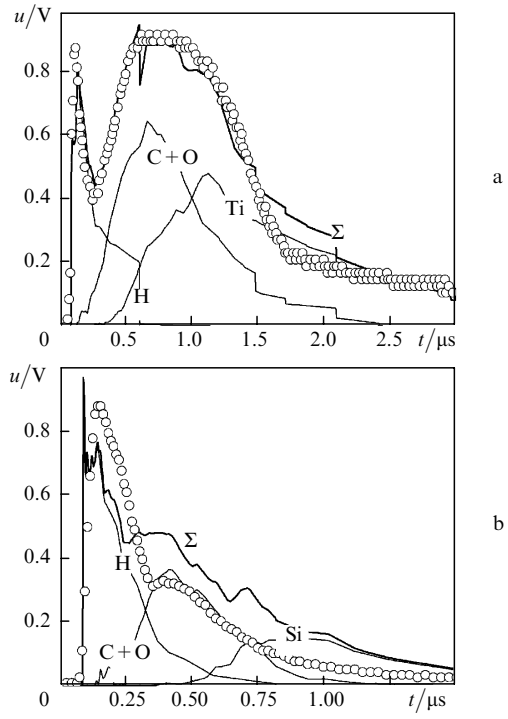

Figure 3. Signals obtained using the time-of-flight technique (○) for (a) Ti and (b) Si targets and reconstructed from the results of mass spectrometric measurements (Σ). Thin solid curves represent partial contributions of different ions.

sponding to propagation velocities of $\sim 2 \times 10^8$ and $\sim 3 \times 10^7$ cm s^{-1}. Figure 3 also shows the time-of-flight spectra reconstructed on the basis of mass-spectrometric data. A mutual normalisation of the spectrum obtained by a direct measurement and a spectrum reconstructed from the data of mass spectrometric measurements was performed at the signal maximum. The coincidence of the leading edges and a satisfactory agreement between the general structures of the ion-current pulses for Ti and Si targets should be noted. Slight differences between the spectra may be due to different voltages at VEU-7 for two techniques that lead to different detection efficiencies for slow ions.

A comparative analysis of the spectra in Fig. 3 shows that the first and second peaks of the ion-current pulse are determined, respectively, by hydrogen and by the sum of the contributions of oxygen, carbon, and the target material. Ions with larger masses acquire lower velocities. Analysing the ion energy spectra shows that protons gain a much higher energy per unit charge (on the average, 9 ± 2 keV) and their acceleration is mainly determined by the hot electron component. The mean energy of this component was evaluated by us at 8 ± 3 keV for both targets also by detecting the yield of hard X-rays. Ions of other atoms are accelerated mainly due to the thermal electron component, whose temperature in our experiments was ~ 250 eV [2].

Hence, the properties of the plasma generated by a femtosecond laser pulse at the solid target surface under our experimental conditions are substantially determined by a surface film consisting of hydrogen, carbon, and oxygen. Note that preliminarily cleaning the interaction region by a femtosecond laser pulse with an intensity $I \sim 10^{12}$ W cm^{-2} leading the main target-irradiating femtosecond pulse by 1 s had no effect on the character of the ion-current pulse envelope.

4. The Si target surface was cleaned using CO_2 laser radiation with an energy density of 10 J cm^{-2} (0.1 GW cm^{-2}). This value was selected on the basis of the following simple estimate of the heated-layer temperature. A temperature increase ΔT in a layer with a thickness L within a time interval τ can be estimated (the specific heat is assumed to be temperature-independent) as

$$\Delta T \approx \frac{W(1-R)}{Lc_p\rho}, \tag{2}$$

where R is the material reflectivity, W is the energy density of the heating laser pulse, and c_p and ρ are the isobaric specific heat and density of the target substance, respectively. The heating depth L is defined as the maximum of the absorption length and the distance to which the heat is transferred for the time τ.

The depth L_t to which a heat wave penetrates during a laser pulse with a duration τ is

$$L_t \sim \left(\frac{\tau\lambda}{c_p\rho}\right)^{1/2}, \tag{3}$$

where λ is the thermal conductivity. The laser-radiation absorption depth can be assessed as

$$L_r \approx \left(\frac{2}{\omega\sigma\varepsilon}\right)^{1/2}, \tag{4}$$

where ω is the laser-radiation frequency; σ is the material conductivity; and ε is the permittivity. The estimated values of L_t and L_r are listed in Table 1.

Analysis of the data of Table 1 shows that, when Si and other materials with a low conductivity are used as targets, a

Table 1. Estimates of the target heating depth and the temperature of the surface layer ΔT for Si and Ti targets irradiated by CO_2 and excimer lasers, respectively.

Target	$\lambda_c/\mu m$	R (%)	$L_t/\mu m$	$L_r/\mu m$	$\Delta T/K$
Si	10.6	36 ± 2	1.5–3	100	500
Ti	0.308	< 8	0.5	0.01	1.5×10^5

rather thick layer at the target surface is heated by 500–1000 °C. Its thickness is determined by the absorption depth and, for silicon heated by CO_2 radiation, is comparable to the Si wafer thickness (300 μm). Thus, the energy density of laser pulses used in the experiment turns out to be sufficient for heating a material layer to a temperature at which the impurity desorption process becomes efficient and a thermal cleaning mode without material melting is observed.

Figure 4 shows ion signals from a plasma formed at cleaned and uncleaned Si target surfaces, when a femtosecond pulse is delayed relative to a CO_2-laser pulse by 100 μs. As a result of surface cleaning, the amplitude of the peak corresponding to hydrogen decreases by a factor of ~ 10. The time of appearance of the second peak slightly increases. This is explained by the fact that the second peak for the uncleaned surface is formed with a participation of not only Si but also C and O. For the cleaned surface, this peak is evidently due to silicon ions. Thus, the target surface is cleaned not only from hydrogen but also from carbon and oxygen. Note that this cleaning mode does not lead to a removal of the oxide layer.

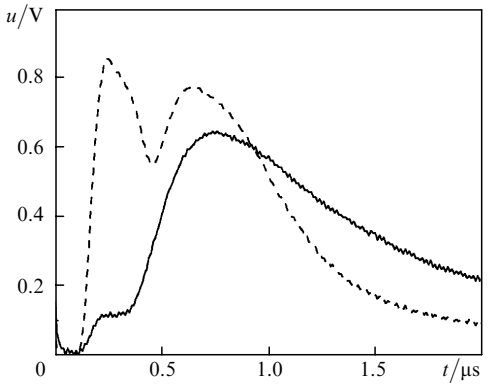

Figure 4. Time-of-flight signals from plasma ions without and with a preliminary Si-target cleaning (dashed and solid curves, respectively) using CO_2-laser radiation (the advance time is $t = 100$ μs).

The delay time between laser pulses was varied using a delay line between 100 μs and 300 ms and manually in the range of 3–10 s. We observed that the surface cleaning quality monitored by the ratio of the first- and second-peak amplitudes changed insignificantly for delays < 100 ms, whereas the cleaning effect disappeared in the manual mode. Thus, the characteristic time of the impurity-layer recovery is < 1 s in this case. Measurements have also shown that the total ion-current value remains constant at any delay times. In addition, the mean energy of the hot electron component measured in the same run of experiments was independent of the presence or absence of a heating nanosecond pulse.

Let us estimate the time of impurity-layer recovery from the residual gas as the time t necessary for the deposition of ten monolayers of particles with a mass M to the target surface with an attachment coefficient $s = 1$ at a pressure of the residual gas p in the chamber. The number of particles that hit the surface with an area S and settle on it within a time t for the Maxwell distribution of particles at a temperature T is

$$N = \frac{1}{2\sqrt{2\pi}} stSn_g \left(\frac{kT}{M}\right)^{1/2}, \quad (5)$$

where $n_g = p/kT$ is the concentration of gas particles and k is the Boltzmann constant. The number of particles in ten layers at the target surface with an area S is $N = 10S(n_s)^{2/3}$, where n_s is the typical density of a solid. Thus,

$$t = \frac{20\sqrt{2\pi}(MkT)^{1/2}}{p} n_s^{2/3}. \quad (6)$$

If a typical particle density in a solid is $n_s = 3 \times 10^{22}$ cm^{-3}, then, for $p = 2 \times 10^{-5}$ Torr, $T = 300$ K, and $M = 1.67 \times 10^{-24}$ kg, the layer deposition time is $t \sim 500$ ms, which has the same order of magnitude as the experimental values.

The Ti-target surface was cleaned with pulsed XeCl laser radiation with an energy density of < 22 J cm^{-2} (0.7 GW cm^{-2}). When Ti or other well-conducting substances are used, the absorption depth (the skin depth) is small and the heated-layer thickness is determined by the heat-transfer depth L_t (see Table 1). Analysis of the tabulated data shows that, when a XeCl laser radiation with an energy density $W \sim 10$ J cm^{-2} is used, the Ti-target surface is broken down and a thin plasma layer with a temperature of 1–10 eV forms. Hence, a plasma target-cleaning mode with a possible removal of the oxide layer is realised. At the same time, estimates of the Ti-target heating should be regarded as upper bounds, since the plasma formation must lead to a substantial increase in the surface reflectivity R.

The ion current of the Ti target was measured using the mass-spectrometry technique. Since the main task of this experiment was to study the efficiency of pulsed laser cleaning of targets as a function of the XeCl laser pulse energy density and the delay time of the femtosecond laser pulse relative to the cleaning pulse, the time-of-flight mass spectrometer was tuned to the region of the ion spectrum corresponding to an ion energy of $1.7Z$ (in keV). In fact, a signal from hydrogen (the energy is 1.7 keV) and other impurity atoms and titanium itself (the energy ranges from 1.7 to 8.5 keV depending on the degree of ionisation) can be observed in this region.

Figure 2b shows a typical form of the signal recorded by the spectrometer for the Ti target, which was preliminarily cleaned by a XeCl-laser pulse that was ahead a femtosecond laser pulse by 90 ns ($W_{CO_2} \sim 20$ J cm^{-2}). As a result of the action of the cleaning laser pulse, the fraction of H, C, and O ions decreases by a factor of 10–20 depending on the type of atoms, the pulse advance time, etc.

With an increase in the advance time t and also with a decrease in the energy flux density W, the cleaning quality gradually lowered. Figure 5 shows the content of the observed elements as a function of the energy density and the advance time. Analysis of these dependences shows that the characteristic rate of the impurity-layer recovery turns out to be higher than when cleaning a Si target by CO_2-laser radiation. For example, in a time of 1–10 ms, the

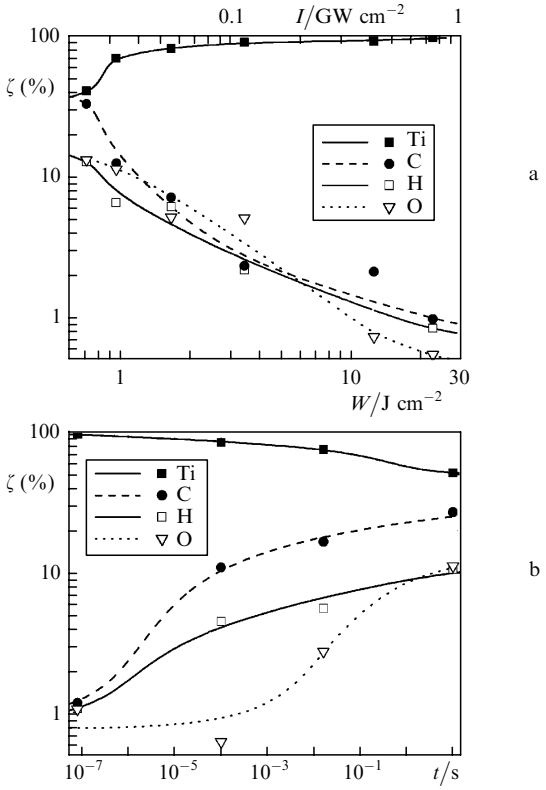

Figure 5. Percentage of ions ζ contained in the ion plasma as a function of (a) the laser energy density W and radiation intensity I at $t = 90$ ns and (b) the time of advance t by which the cleaning XeCl-laser pulse is ahead of the plasma-generating pulse for $W = 22$ J cm^{-2} (Ti target).

total amount of impurities reaches half the initial quantity, while the degree of cleaning using CO_2-laser radiation remained unchanged for an advance time of < 100 ms.

The process of the impurity-layer recovery has the maximum rate for hydrogen and carbon, while the oxygen recovery rate is 1000 times lower. The recovery times (at a level of 1/e) are $t_H \sim 300$ μs for hydrogen, $t_C \sim 100$ μs for carbon, and $t_O \sim 100$ ms for oxygen (Fig. 5b). A decrease in the recovery time, which is observed for the Ti target, compared to the Si target may be associated with the recovery of an impurity layer at the Ti-target surface due to a diffusion of H atoms from the target depth. In fact, the hydrogen diffusion speed in Ti and Si at $T = 500 - 1500$ °C is $D_0 \sim 10^{-2} - 10^{-3}$ cm^2 s^{-1} [24]; i.e., the H diffusion distance is 3–10 μm for 100 μs. This value exceeds the depth of Ti warming-up (1 μm) by UV radiation from an excimer laser but is significantly smaller than the depth to which the Si target is heated by CO_2-laser radiation (Table 1). Thus, the fast recovery of an impurity layer at the Ti-target surface may be related to a diffusion of hydrogen and other impurities from the target depth.

Measurements performed for the Ti target at the minimum advance time (100 ns) have shown that, under such cleaning conditions, a significant fall of the H, C, and O ion current and a certain decrease in the signal due to Ti ions are observed. The ratio between the total ion currents measured with and without a cleaning pulse as a function of the delay time between two laser pulses is plotted in Fig. 6. A signal decrease is evidently associated with absorption of the femtosecond laser pulse in the low-density plasma formed by the nanosecond laser pulse. This result complies with the above estimate of the temperature to which the surface layer is heated. This estimate demonstrates the possibility of forming plasma in this irradiation mode. Thus, the optimal delay time of the plasma-generating pulse relative to the cleaning pulse in this interaction mode is 10–100 μs.

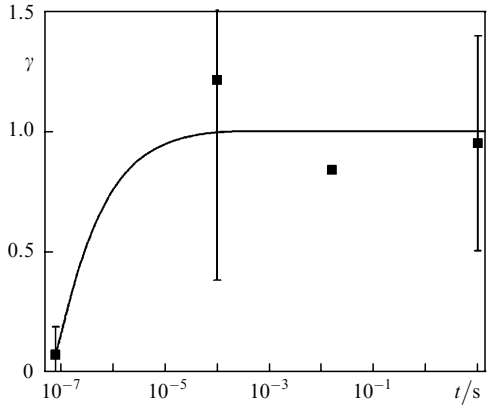

Figure 6. Ratio γ between the total ion currents measured with and without a cleaning pulse as a function of the delay time between the cleaning and plasma-generating laser pulses (a Ti target is cleaned by XeCl-laser pulses with an energy density $W = 22$ J cm^{-2}).

The threshold energy density necessary for an efficient removal of impurity atoms from the target surface is 1–3 J cm^{-2} (Fig. 5a). In this case, melted areas 200–250 μm in diameter appeared at the target surface. This threshold differs for different atoms: the energy-density values necessary for removing impurities are $W_H \sim 1$ J cm^{-2} for hydrogen, $W_C \sim 2$ J cm^{-2} for carbon, and $W_O \sim 3$ J cm^{-2} for oxygen (Fig. 5a). An effect of impeded oxygen removal observed earlier in Refs [14, 15] can be explained by the presence of oxygen in the form of a chemically stable oxide layer. Hence, the optimal energy density of the cleaning laser pulse is 3–10 J cm^{-2}.

An interesting feature is the appearance of a spectral peak in Fig. 2b whose time position corresponds to a particle with a mass $M = 96$ and a charge of 1, which may correspond to the $Ti^{1+} - Ti^0$ cluster. In Fig. 2a, this peak is at a level of the noise background.

5. We have shown that the acceleration of ions in the plasma generated by a 2×10^{16} W cm^{-2} femtosecond laser pulse on the surface of a solid target at a pressure of up to 10^{-5} Torr is appreciably affected by an impurity film containing hydrogen, carbon, and oxygen atoms. Under such conditions, the highest mean energy per unit charge (8.5 keV) is gained by the protons accelerated by the hot plasma electron component, while the ions constituting the target material (Si or Ti in our experiments) are accelerated at the expense of the thermal electron component with an energy per unit charge of < 1 keV. When using the time-of-flight measurement technique for analysing the energy spectrum of the ions accelerated in the high-temperature near-surface plasma in a vacuum chamber with an average residual pressure of $\sim 10^{-5}$ Torr, one should allow for the fact that the first (fast) current pulse is related to a proton emission from the target surface.

By using a nanosecond laser pulse with an energy density of < 10 J cm^{-2} that has a controlled advance of 100 μs–100 ms relative to a femtosecond laser pulse, it is possible to

control the number of laser-induced high-energy protons and efficiently clean the target surface by removing H-, C-, and O-containing molecules from it. Unlike a continuous thermal surface heating, the pulse laser cleaning provides high heating temperatures and can be efficiently applied to any solid target.

A molecular layer at the target surface at a pressure of 10^{-5} Torr recovers through an adsorption from the residual gas within a time of > 100 ms. Thus, to ensure the interaction of the femtosecond laser pulse with the 'clean' surface, the nanosecond and femtosecond pulses must be synchronised so that the delay time of the latter relative to the former should not exceed 100 ms in the thermal-cleaning regime and be in the range of 100 ns – 100 μs in the plasma-cleaning regime.

The impurity layer of hydrogen and other atoms can also be restored through a diffusion of impurity atoms from the target depth. This effect may become especially significant if the residual pressure in the interaction chamber lowers to 10^{-7}–10^{-9} Torr. The diffusive mechanism of the impurity-layer recovery can be partially suppressed when using IR radiation of a CO_2 laser.

Acknowledgements. This work was supported by the Russian Foundation for Basic Research (Grant No. 02-02-16659) and the International Science and Technology Center (Grant No. 2651p).

References

1. Volkov R.V., Gordienko V.M., Lachko I.M., et al. *Pis'ma Zh. Eksp. Teor. Fiz.*, **76**, 171 (2002).
2. Gordienko V.M., Lachko I.M., Mikheev P.M., et al. *Plasma Physics and Controlled Fusion*, **44**, 2555 (2002).
3. Hegelich M., Karsch S., Pretzler G., et al. *Phys. Rev. Lett.*, **89**, 85002 (2002).
4. Badziak J., Woryna W., Parys P., et al. *Phys. Rev. Lett.*, **87**, 215001 (2001).
5. Maksimchuk A., Gu S., Flippo K., et al. *Phys. Rev. Lett.*, **84**, 4108 (2000).
6. Clark E.L., Krushelnuk K., Zepf M., et al. *Phys. Rev. Lett.*, **85**, 1654 (2000).
7. Gitomer S.J., Jones R.D., Begay F., et al. *Phys. Fluids*, **29**, 2679 (1986).
8. Zehner D.M., White C.W., Ownby G.W. *Appl. Phys. Lett.*, **36**, 56 (1980).
9. Meyerhofer D.D., Chen H., Delettrez J.A., et al. *Phys. Fluids B*, **5**, 2584 (1993).
10. Andreev A.A., Gamalii E.G., Novikov V.N., et al. *Zh. Eksp. Teor. Fiz.*, **101**, 1808 (1992).
11. Volkov R.V., Golishnikov D.M., Gordienko V.M., et al. *Pis'ma Zh. Eksp. Teor. Fiz.*, **72**, 577 (2000).
12. Ehler W., Begay F., Tan T.H., et al. *J. Phys. D*, **13**, L29 (1980).
13. Begay F., Forslund D.W. *Phys. Fluids*, **25**, 1675 (1982).
14. Tsu R., Lubben D., Bramblett T.R., et al. *J. Vacuum Sci. & Tech. A*, **9**, 223 (1991).
15. Watanabe J.K., Gibson U.J. *J. Vacuum Sci. & Tech. A*, **10**, 823 (1992).
16. Zheng Y.W., Luk'ynchuk B.S., Lu Y.F., et al. *J. Appl. Phys.*, **90**, 2135 (2001).
17. Lu Y.F., Zheng Y.W., Song W.D. *J. Appl. Phys.*, **87**, 1534 (2000).
18. Volkov R.V., Gordienko V.M., Dzhidzhoev M.S., et al. *Kvantovaya Elektron.*, **24**, 1114 (1997) [*Quantum Electron.*, **27**, 1081 (1997)].
19. Volkov R.V., Gordienko V.M., Mikheev P.M., et al. *Kvantovaya Elektron.*, **30**, 896 (2000) [*Quantum Electron.*, **30**, 896 (2000)].
20. Volkov R.V., Gavrilov S.A., Golishnikov D.M., et al. *Kvantovaya Elektron.*, **31**, 241 (2001) [*Quantum Electron.*, **31**, 241 (2001)].
21. Golishnikov D.M., Gordienko V.M., Savel'ev A.B., et al. *Proc. SPIE Int. Soc. Opt. Eng.*, **4752**, 221 (2002).
22. Golishnikov D.M., Gordienko V.M., Mikheev P.M., et al. *Laser Phys.*, **11**, 1205 (2001).
23. Ageev V.P., Gorbunov A.A., Danilov V.P., et al. *Kvantovaya Elektron.*, **10**, 2451 (1983) [*Sov. J. Quantum Electron.*, **13**, 1595 (1983)].
24. Grigor'ev I.S., Meilikhov E.Z. (Eds) *Fizicheskie velichiny. Spravochnik* (Handbook of Physical Quantities) (Moscow: Energoatomizdat, 1991) p. 378.